

Learning to embed semantic similarity for joint image-text retrieval

Noam Malali and Yosi Keller



Abstract—We present a deep learning approach for learning the joint semantic embeddings of images and captions in a Euclidean space, such that the semantic similarity is approximated by the L_2 distances in the embedding space. For that, we introduce a metric learning scheme that utilizes multitask learning to learn the embedding of **identical** semantic concepts using a center loss. By introducing a differentiable quantization scheme into the end-to-end trainable network, we derive a semantic embedding of semantically **similar** concepts in Euclidean space. We also propose a novel metric learning formulation using an adaptive margin hinge loss, that is refined during the training phase. The proposed scheme was applied to the MS-COCO, Flickr30K and Flickr8K datasets, and was shown to compare favorably with contemporary state-of-the-art approaches.

Index Terms—Text and Image Fusion, Deep Learning, Joint Embedding

1 INTRODUCTION

The joint embedding of text and image data is a contemporary research theme paving the way for novel applications such as Visual Question Answering [1], auto-caption generation [2], and image-to-text retrieval [3] [4]. Figure 1 depicts image-to-text retrieval where a query image is embedded in a joint image-text space, and the chosen caption is the one closest to the image in terms of their L_2 distance, in the joint embedding space. Similarly, given a caption, the joint embedding space allows text-to-image retrieval, where the closest image is retrieved. The computation of the joint embedding space is commonly formulated as a Metric Learning problem using training sets of corresponding images and captions.

Let the image and caption, be denoted by \mathbf{x} and \mathbf{y} , respectively. We aim to compute their corresponding joint embedding $\hat{\mathbf{x}}, \hat{\mathbf{y}} \in \mathbb{R}^d$, using the mapping functions \mathbf{H}_i and \mathbf{H}_t , respectively, such that

$$\hat{\mathbf{x}}_n = \mathbf{H}_i(\mathbf{x}_n), \hat{\mathbf{y}}_n = \mathbf{H}_t(\mathbf{y}_n) \quad (1)$$

The mappings $\{\mathbf{H}_i, \mathbf{H}_t\}$ are learned using a supervised scheme, given a training set of $S = \{\mathbf{x}_i, \mathbf{y}_i\}_1^N$ samples, and corresponding binary labels. In practice, S only consists of semantically identical pairs, while all other pairs are



1. Six People riding bikes on a trail in the forest.
2. There are six men mountain biking in a forest terrain.
3. Six people ride mountain bikes through a jungle environment.
4. A group of mountain bikers race each other down a dirt hill.
5. A group of people is bike riding in the woods.
6. Bicycle rider wearing black, riding down a dirt trail in a mountain bike.
7. **Men, surrounded by nature, are riding mountain bikes.**
8. A group of kids on their bicycles smiling at the photographer on a dirt trail.
9. Some nature hikers stop to examine a log along the path.
10. Two people riding bikes through a mountainous region.

Fig. 1. Image caption retrieval (image to text), using the Flickr30K dataset [5]. The embedding of an image is compared with the embedding of all sentences in the dataset, and the closest ten captions are presented. The sentences marked in bold are the ground truth matches having *identical* semantic content, in contrast to the other sentences having *similar* content.

considered dissimilar. $\{\mathbf{H}_i, \mathbf{H}_t\}$ are learned to optimize a distance metric, such as L_1 and L_2 , over the training set.

Metric learning was applied in a plethora of problems and classical formulations [6], [7]. In this work, we relate to metric learning in the context of joint image-text embeddings, where several schools of thought were studied. Some schemes utilize only similar pairs to increase the correlation between their embeddings, based on variants of Canonical Correlation Analysis (CCA) [8] such as KCCA [9], and their extensions using Convolutional Neural Networks (CNNs), such as the 2WayNet [10], DCCA [11] and CorrNet [12].

Other approaches, such as Visual Semantic Embedding (VSE++) [13], Dual Attention Network (DAN) [14], sm-LSTM [15] and Embedding Network [16] utilize both similar and dissimilar pairs to minimize the distance of the similar pairs in the embedding space, while maximizing the distance of the dissimilar ones. In the Contrastive loss a hinge loss is applied to the distance metric of dissimilar samples

$$\mathcal{L}_p = \sum_{n=1}^N D(\hat{\mathbf{x}}_n, \hat{\mathbf{y}}_n^+) + \sum_{n=1}^N [m - D(\hat{\mathbf{x}}_n, \hat{\mathbf{y}}_n^-)]_+ \quad (2)$$

where $\{\hat{\mathbf{x}}_n, \hat{\mathbf{y}}_n^+\}$ and $\{\hat{\mathbf{x}}_n, \hat{\mathbf{y}}_n^-\}$ are a pair of embeddings of similar and dissimilar samples, respectively, and $[x]_+ = \max(x, 0)$. m is predefined, and it is common to set $m = 1$ for L_2 normalized embeddings. A Triplet Loss [17] optimizes the difference in distances between similar $\{\hat{\mathbf{x}}_n, \hat{\mathbf{y}}_n^+\}$ and dissimilar $\{\hat{\mathbf{x}}_n, \hat{\mathbf{y}}_n^-\}$ pairs

$$\mathcal{L}_T = \sum_{n=1}^N [D(\hat{\mathbf{x}}_n, \hat{\mathbf{y}}_n^+) - D(\hat{\mathbf{x}}_n, \hat{\mathbf{y}}_n^-) + m]_+, \quad (3)$$

• N. Malali & Y. Keller are with the Faculty of Engineering, Bar-Ilan University, E-mail: yosi.keller@gmail.com

Manuscript received April 19, 2005; revised August 26, 2015.

where $\{\hat{\mathbf{x}}_n, \hat{\mathbf{y}}_n^+, \hat{\mathbf{y}}_n^-\}$ is a triplet of samples such that $\hat{\mathbf{x}}_n$ is an image embedding, while $\hat{\mathbf{y}}_n^+$ and $\hat{\mathbf{y}}_n^-$ are semantically similar and dissimilar captions, respectively.

Recent works [18], [19], [20] applied bottom-up attention schemes, where the image is semantically parsed, and the resulting ROIs are matched to the captions. The ROIs are detected by Faster RCNN [21]. The number of dissimilar pairs far exceeds that of similar ones, and as most dissimilar pairs are easy to detect, they prove uninformative for training. Thus, informative dissimilar samples denoted as *hard negatives* have to be chosen explicitly.

In this work, we formulate the image-text embedding as the embeddings of semantically *identical* and *similar* images and captions. The sets of semantically *identical* images and captions are given by the training sets $S = \{\mathbf{s}_n\}_1^N = \{\mathbf{x}_n, \mathbf{y}_n^1, \dots, \mathbf{y}_n^K\}_1^N$ [5], [22], [23]. Each subset \mathbf{s}_n consists of an image \mathbf{x}_n and K corresponding (semantically identical) captions $\mathbf{y}_n^1, \dots, \mathbf{y}_n^K$. We propose to quantize the semantic embeddings using an end-to-end deep learning scheme, to derive an embedding that relates *similar* images and captions, that are not given by the training sets. The joint embedding is computed by applying a network consisting of two embedding branches. The first computes the image representation using convolution layers, while the second computes the text embedding using word embedding and GRU layers, as depicted in Fig. 2. As identical samples are a subset of the similar ones, we propose a novel approach to separately induce the similarity of identical and similar images and captions, such that the similarity of identical samples is increased compared to that of the similar ones.

Thus, the proposed CNN is trained using multitask learning. We apply a the proposed Semantic Center Loss to compute the semantic embedding and induce the similarity of *similar* samples, and a novel formulation of the Triplet Loss, using an adaptive-margin, to induce the similarity of *identical* samples. Cross-entropy losses are applied to each of the image and text embedding branches separately, to improve their convergence. The proposed semantic embedding and Triplet Loss formulation can be used with *any* CNN backbone implementing the image and text embeddings.

In particular, we propose the following contributions:

First, we present a CNN-based joint image-text embedding scheme to learn a semantic representation using training sets of images and captions encoding *identical* semantic notions.

Second, by quantizing the resulting semantic embeddings using an end-to-end deep learning approach, we agglomerate the semantic representation to derive an embedding that encodes semantic *similarity* in terms of L_2 distances in the embedding space.

Third, we propose a novel Triplet Loss formulation that utilizes a hinge loss with adaptive margins that is shown to improve the embedding accuracy.

Last, the proposed scheme is shown to compare favorably with contemporary state-of-the-art approaches when applied to the retrieval of images given their corresponding captions, and vice versa.

2 BACKGROUND

Metric learning is a fundamental topic in machine learning applied in a plethora of problems and classical formulations [6], [7], and was used in joint image-text embeddings.

Klein et al. [8] applied Canonical Correlation Analysis (CCA), to compute a linear projection of two data views into a joint space that maximizes the correlation between their embeddings. CCA utilizes only positive pairs of samples and has been applied by Li et al. [24] to face recognition, and by Klein et al. [8] for relating text to images. A Deep canonical correlation analysis (DCCA) was proposed by Andrew et al. [11], where CCA was used as a loss function.

Other deep learning schemes such as Correlation Neural Networks (CorrNet) by Chandar et al. [12] and DCCAE by Wang et al. [25] utilized an autoencoder architecture with two input and output views. Contemporary Deep CCA methods optimize the CCA loss on top of a CNN. Thus, Eisenschtat and Wolf [10] introduced the 2Way Network architecture consisting of a bidirectional CNN that was optimized using an L_2 loss, to match the two data sources. Another widely used approach is the ranking hinge loss, which utilizes positive/similar and negative/dissimilar data pairs, to learn a representation in which the positive pairs are closer than negative ones. A pairwise hinge ranking loss was applied by Chechik et al. [26] for learning image similarity and similarity-preserving hash functions. Similarly, Norouzi and Fleet [27] studied the embedding of high dimensional data as binary codes.

Pairwise losses were applied to image-text metric learning by Weston et al. [28] for the annotation of large scale image datasets. A ranking hinge loss for deep visual semantic embedding was applied by Frome et al. [29] to improve the identification, and recognition of visual objects. Kiros et al. [3] proposed to apply the triplet ranking loss to visual semantic embedding and image captioning. The same loss was also used by Karpathy et al. [4] and Socher et al. [30] to generate natural language captioning of images. The learning of similarity embedding using CNN was suggested by Wang et al. [16] by applying a maximum-margin triplet ranking loss. Hard Mining was shown to improve CNN training in general, and metric learning in particular by Faghri et al. [13]. Image-text similarity was formulated as a binary classification problem by Jabri et al. [31] for Visual Question Answering (VQA), to predict the matching of images and questions. The same loss was used in a zero-shot formulation by Ba et al. [32] to match images and captions using a CNN consisting of two CNN subnetworks. The accuracy of metric learning-bases was improved by Wu et al. [33] by introducing an adaptive margin into the Hinge loss within the Contrastive loss, as in Eq. 2. The adaptive margin is optimized during the training phase. Similarly, Chen [34] proposed an adaptive margin based on the average distance between the positive and negative training samples, to improve the proposed quadruplet metric learning scheme. A class-adaptive margin loss was proposed by Li et al. [35], where semantic similarity between each pair of classes was analyzed to separate samples from similar classes in the embedding domain. The proposed margin was applied to improve the generalization of meta-learning in few-shot learning problems.

Attention-based approaches [18], [19], [20] applied Bottom-up visual parsing to match images and captions, where the set of semantic concepts is represented by a vocabulary of words derived by analyzing the captions in the training set. The training images were visually parsed by extracting multiple ROIs from each image using the Region Proposal Network (RPN) of the Faster R-CNN [21], and associating semantic concepts as attributes per ROI. Huang et al. [18] utilize a multi-label CNN to predict the semantic concepts per ROI, that are merged, and fused with a global image context, resulting in a joint embedding. Lee et al. [19] applied stacked cross attention to match the ROIs estimated by the bottom-up image parsing, to words, to derive a one-to-one matching scheme without computing a joint embedding in an L_2 space. Li et al. [20] extended these schemes by applying Graph Convolutional Networks (GCN) to the embeddings of the extracted ROIs, to derive features with semantic relationships and the multiple ROI embeddings were fused using an RNN. This approach achieved state-of-the-art accuracy. In addition to a training set of semantically identical images and captions (MS-COCO, Flickr30K), such schemes require a large-scale annotated set of instances ('building,' 'giraffe,' etc.) and attributes ('furry,' 'fast,' etc.) appearing in the images, to train the Faster RCNN [21]. The *Support-set* work [36] by Patrick et al. is of particular interest, as it studies the joint embedding of video sequences and text. Patrick et al. propose a center loss with soft assignments, whose centers are chosen from the embeddings of the frames of the video sequence. Thus, the embedding of each caption is a linear combination of the embeddings of the Support-set video frames.

3 JOINT SEMANTIC EMBEDDING OF IMAGES AND CAPTIONS

Let $S = \{s_n\}_1^N = \{\mathbf{x}_n, \mathbf{y}_n^1, \dots, \mathbf{y}_n^K\}_1^N$ be a set of subsets s_n each consisting of an image \mathbf{x}_n and K captions $\{\mathbf{y}_n^1, \dots, \mathbf{y}_n^K\}$. We aim to compute the joint embeddings of S

$$\hat{S} = \{\hat{\mathbf{x}}_n, \hat{\mathbf{y}}_n^1, \dots, \hat{\mathbf{y}}_n^K\}_1^N, \hat{\mathbf{x}}_n, \hat{\mathbf{y}}_n^k \in \mathbb{R}^d \quad (4)$$

such that the embeddings \hat{S} encode the semantic similarities of S , by minimizing the L_2 distances between semantically similar images and captions, and maximizing the distances between semantically dissimilar ones.

Sets of semantically *identical* images and captions S are given in the Flickr8K [22], Flickr30K [5], and MS-COCO [23] training sets. Each of these training datasets S consists of subsets s_n containing a single image and $K = 5$ corresponding captions that encode an *identical* semantic concept.

3.1 Network Backbone

The outline of the proposed CNN is shown in Fig. 2. The proposed scheme consists of image and text embedding branches, H_i and H_t , respectively, that compute the image and text embeddings $\hat{\mathbf{x}}_n$ and $\hat{\mathbf{y}}_n$. We used *multiple* different backbone architectures, to compare against recent results as reported in Section 4. All different backbones compute (differently) the image and text embeddings $\hat{\mathbf{x}}_n$ and $\hat{\mathbf{y}}_n$, as in Fig. 2, while the rest of the proposed network, that is the core of our contribution, is detailed in Section 3.2.

Figure 2 shows a backbone following 2WayNet [10] and VSE++ [13], where the input image \mathbf{x}_n is embedded by VGG19 or ResNet152 CNNs. An FC layer adjusts the output dimensionality of the image embeddings $\hat{\mathbf{x}}_n$ to that of the text embeddings $\hat{\mathbf{y}}_n$. The text embedding is computed by an embedding layer followed by a GRU layer. We also used the Attention-based backbone proposed by the (previous) SOTA VSRN approach [20] by Li et al.

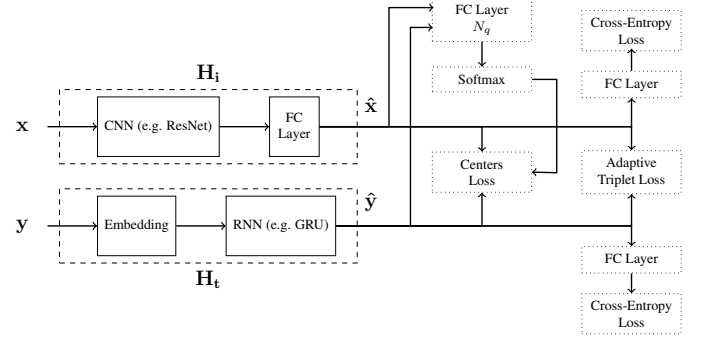


Fig. 2. The proposed joint embedding scheme. The outputs of the image and text branches are $\hat{\mathbf{x}}$ and $\hat{\mathbf{y}}$, respectively. We used multiple different backbones. The backbone shown follows [10], [13]. The subnetwork to the right of $\hat{\mathbf{x}}$ and $\hat{\mathbf{y}}$ is common to *all* our architectures, and is the *core* of our approach. $\hat{\mathbf{x}}$ and $\hat{\mathbf{y}}$ are connected to separate cross-entropy losses labeled by their given set s_n . A triplet hinge loss with adaptive margins, as in Section 3.5, is used to merge the embeddings. The *unquantized* embedding is computed by directly connecting $\hat{\mathbf{x}}$ and $\hat{\mathbf{y}}$ to the Center Loss as in Section 3.3, to compute the semantic centers $\{c_n\}_1^N$. For the *quantized* embedding as in Section 3.4, $\hat{\mathbf{x}}$ and $\hat{\mathbf{y}}$ are connected to the " N_q FC" and Softmax layers to compute $N_q \ll N$ embedding centers $\{\hat{c}_n\}_1^{N_q}$.

3.2 Semantic Embedding Subnetwork

Given the image and text embeddings $\hat{\mathbf{x}}_n$ and $\hat{\mathbf{y}}_n$, as in Fig. 2, the Semantic embedding subnetwork (to the right of $\hat{\mathbf{x}}_n$ and $\hat{\mathbf{y}}_n$ in Fig. 2) is shared by *all* of our proposed schemes and is the *core* of our contribution. The semantic embedding of identical subsets s_n is learned by applying the Semantic Center Loss \mathcal{L}_C , detailed in Section 3.3 to minimize the inner-set variance of the embedding \hat{s}_n of the subsets s_n . Different training subsets $\{s_n\}$ might encode *similar* (not identical) semantic concepts. But, the semantic similarity is not given by the training sets. To compute an embedding that encodes semantic similarity, we propose to quantize the embeddings $\{\hat{s}_n^i\}$ using $N_q \ll N$ semantic centers as discussed in Section 3.4. This allows to agglomerate N identical concepts to N_q similar concepts.

We also apply a novel formulation of the Triplet Hinge Loss \mathcal{L}_T detailed in Section 3.5, that utilizes adaptive hinge loss margins. The margins are updated during the training and allow better separation (in the L_2 sense) of the different semantic concepts.

Last, we apply two separate cross-entropy (CE) losses, \mathcal{L}_{CE}^I and \mathcal{L}_{CE}^T , for the image and text embeddings, respectively. These losses classify each embedding $\hat{\mathbf{x}}_n \in s_n$ or $\hat{\mathbf{y}}_n \in s_n$ with respect to the index n of its subset s_n . As $S = \{s_n\}_1^N$, there are N such classes. The overall loss is the unweighted sum of all losses above

$$L = \mathcal{L}_C + \mathcal{L}_T + \mathcal{L}_{CE}^I + \mathcal{L}_{CE}^T. \quad (5)$$

We experimented in weighing the different loss, but the accuracy was not improved.

3.3 Semantic Center Loss

Each subset $s_n = \{\mathbf{x}_n, \mathbf{y}_n^1, \dots, \mathbf{y}_n^K\}$ in the given training sets [5], [22], [23] consists of semantically *identical* entries. Let $\mathbf{c}_n \in \mathbb{R}^d$ be the embedding (semantic center) corresponding to the subset s_n . \mathbf{c}_n and s_n are apriori assigned and we have $C = \{\mathbf{c}_n\}_1^N$ semantic centers that are learned in the training phase. The *same* embedding center \mathbf{c}_n is applied to the embeddings of *both* image and captions training entries $\{\mathbf{x}_n, \mathbf{y}_n^1, \dots, \mathbf{y}_n^K\} \in s_n$, as both are given to be semantically identical.

We propose to minimize the Center Loss [37] with respect to both images and captions

$$\mathcal{L}_C = \sum_i (\|\hat{\mathbf{x}}_i - \mathbf{c}_{(\hat{\mathbf{x}}_i, \hat{\mathbf{y}}_i)}\|_2^2 - \delta)_+ + (\|\hat{\mathbf{y}}_i - \mathbf{c}_{(\hat{\mathbf{x}}_i, \hat{\mathbf{y}}_i)}\|_2^2 - \delta)_+ \quad (6)$$

where $\mathbf{c}_{(\hat{\mathbf{x}}_i, \hat{\mathbf{y}}_i)}$ is the center corresponding to both $\hat{\mathbf{x}}_i$ and $\hat{\mathbf{y}}_i$, respectively. During training, the proposed CNN is given triplets of input images and captions used for the metric learning detailed in Section 3.5, and the Center Loss \mathcal{L}_C is minimized for each image and caption training sample.

3.4 Quantized Semantic Center Loss

The Center Loss in Eq. 6 minimizes the inner variability of each subset $s_n \in S$. But, the resulting embedding does not minimize the L_2 distance between the embeddings of semantically *similar* (but not identical) images and corresponding captions. Moreover, with the use of large training sets, such as the MS-COCO [23] dataset, the number of subsets $|S| = N$ and corresponding centers \mathbf{c}_n increases significantly, to $N > 100K$, implying that many of the semantic concepts encoded by the training sets S are similar. Thus, the semantic centers $\{\mathbf{c}_n\}_1^N$, computed in Section 3.3, can be quantized to derive an embedding that encodes *semantic similarity*, such that the samples in semantically similar sets s_n will have a similar embedding in the L_2 metric.

Hence, we propose to quantize the semantic centers $\{\mathbf{c}_n\}_1^N$ to $C_q = \{\hat{\mathbf{c}}_n\}_1^{N_q}$, $N_q \ll N$, by applying a *soft* differentiable quantization scheme, where a Softmax layer is utilized to assign soft labels [38]. The soft assignments $\mathbf{w}_{\hat{\mathbf{x}}_i}, \mathbf{w}_{\hat{\mathbf{y}}_i} \in \mathbb{R}^{N_q}$ are computed by applying the Softmax layer to $\hat{\mathbf{x}}_i$ (image) and $\hat{\mathbf{y}}_i$ (text), respectively.

Given the soft assignments to the quantized semantic centers C_q , the centers are learned using an extension of the Semantic Center Loss [39].

$$\begin{aligned} \mathcal{L}_C = & \sum_i \sum_{j=1}^{N_q} \mathbf{w}_{\hat{\mathbf{x}}_i}(\mathbf{c}_j) (\|\hat{\mathbf{x}}_i - \hat{\mathbf{c}}_j\|_2^2 - \delta)_+ \\ & + \sum_i \sum_{j=1}^{N_q} \mathbf{w}_{\hat{\mathbf{y}}_i}(\mathbf{c}_j) (\|\hat{\mathbf{y}}_i - \hat{\mathbf{c}}_j\|_2^2 - \delta)_+ \\ & + \alpha \sum_{k_1, k_2}^{N_q} \left(2\delta - \|\hat{\mathbf{c}}_{k_1} - \hat{\mathbf{c}}_{k_2}\|_2^2 \right)_+, \quad (7) \end{aligned}$$

where $\mathbf{w}_{\hat{\mathbf{x}}_i}(\mathbf{c}_j)$ and $\mathbf{w}_{\hat{\mathbf{y}}_i}(\mathbf{c}_j)$ are the soft assignment weights of the sample $\hat{\mathbf{x}}_i$ and $\hat{\mathbf{y}}_i$ to the center \mathbf{c}_j , and $\alpha > 0$ is a weight term that was set to $\alpha = 1$. Note that as $\mathbf{w}_{\hat{\mathbf{x}}_i}$ and $\mathbf{w}_{\hat{\mathbf{y}}_i}$ are the outputs of a Softmax layer, we have that

$$\sum_{j=1}^{N_q} \mathbf{w}_{\hat{\mathbf{x}}_i}(\mathbf{c}_j) = 1, \forall \hat{\mathbf{x}}_i \quad (8)$$

and

$$\sum_{j=1}^{N_q} \mathbf{w}_{\hat{\mathbf{y}}_i}(\mathbf{c}_j) = 1, \forall \hat{\mathbf{y}}_i. \quad (9)$$

Thus, Eq. 7 implies that both $\hat{\mathbf{x}}_i$ and $\hat{\mathbf{y}}_i$ are reconstructed as a linear combination of the quantized centers $C_q = \{\hat{\mathbf{c}}_n\}_1^{N_q}$.

In this formulation, the Center Loss in Eq. 6 is extended by adding a term that pushes the centers away from each other, to improve the separability of the embeddings of centers that are semantically dissimilar. As the training sets only provide semantically identical subsets s_n , it is apriori unknown whether different training subsets s_{n_1} and s_{n_2} , $n_1 \neq n_2$ are similar or dissimilar. Thus, the additional term in Eq. 7 could not be used without applying the differentiable semantic quantization that introduces the notion of semantic dissimilarity. Equation 7 does not distinguish between similar and identical samples, as similar samples are a superset of the identical ones. In order to further induce the similarity of identical samples we apply the Triplet Hinge Loss detailed in Section 3.5.

3.5 Triplet Hinge Loss with Adaptive Margins

The hinge loss is widely used in metric learning schemes as in Eqs. 2 and 3. It is common to set $m = 1$ for L_2 normalized embeddings, and it provides adaptive Hard Negative Mining, discarding negative samples with classification margins larger than m , which are often uninformative.

We propose an adaptive margin m that is updated throughout the training iterations. Starting with a relatively small threshold m , corresponding to a weak separation of negative samples, and adaptively increasing m as the separation improves due to the CNN training.

We apply the adaptive margin to a symmetric Triplet Loss formulation as in Eq. 3

$$\begin{aligned} \mathcal{L}_T = & \sum_{n=1}^N [D(\hat{\mathbf{x}}_n, \hat{\mathbf{y}}_n^+) - D(\hat{\mathbf{x}}_n, \hat{\mathbf{y}}_n^-) + m_x]_+ \\ & + \sum_{n=1}^N [D(\hat{\mathbf{y}}_n, \hat{\mathbf{x}}_n^+) - D(\hat{\mathbf{y}}_n, \hat{\mathbf{x}}_n^-) + m_y]_+ \quad (10) \end{aligned}$$

where $\{\hat{\mathbf{x}}_n, \hat{\mathbf{y}}_n^+, \hat{\mathbf{y}}_n^-\}$ is a triplet of samples such that $\hat{\mathbf{x}}_n$ is an image embedding, while $\hat{\mathbf{y}}_n^+$ and $\hat{\mathbf{y}}_n^-$ are identical and non-identical captions, respectively, as given in the training sets. The triplet $\{\hat{\mathbf{y}}_n, \hat{\mathbf{x}}_n^+, \hat{\mathbf{x}}_n^-\}$ is the symmetric counterpart of the text embedding $\hat{\mathbf{y}}_n$. m_x and m_y are the adaptive margins for the image and text branches, respectively, and N is the number of negative and positive samples.

m_x and m_y are updated every q batches, by computing the ratios M_x and M_y , of negative samples (within the batch) adhering to the margins m_x and m_y

$$M_x = \frac{1}{N} \sum_{n=1}^N \#[D(\hat{\mathbf{x}}_n, \hat{\mathbf{y}}_n^+) - D(\hat{\mathbf{x}}_n, \hat{\mathbf{y}}_n^-) + m_x > 0], \quad (11)$$

$$M_y = \frac{1}{N} \sum_{n=1}^N \#[D(\hat{\mathbf{y}}_n, \hat{\mathbf{x}}_n^+) - D(\hat{\mathbf{y}}_n, \hat{\mathbf{x}}_n^-) + m_y > 0]. \quad (12)$$

$M_x > r$ or $M_y > r$ implies that the CNN can separate a sufficient ratio of the negative samples, and the margins m_x and m_y can be increased to induce a stronger separation. Thus, the margins m_x and m_y are updated by

$$m_{x,y} = \begin{cases} c \cdot m_{x,y} & \text{if } M_{x,y} > r \\ m_{x,y}, & \text{otherwise.} \end{cases} \quad (13)$$

where $c > 1$ is a predefined update multiplier.

Equations 11-13 are applied every q batches to allow a statistically stable estimate of $M_{x,y}$.

4 EXPERIMENTAL RESULTS

The proposed scheme was experimentally verified by applying it to multiple contemporary image-text datasets used in previous state-of-the-art schemes. We used the Flickr8K [22], Flickr30K [5], MS-COCO [23] datasets, consisting of 8,000, 31,000 and 123,000 images, respectively, where each image was annotated by five captions. Thus, for each training dataset, we are given $\{s_n\}_1^N$ training sets, each consisting of $s_n = \{\mathbf{x}_n, \mathbf{y}_n^1, \dots, \mathbf{y}_n^5\}$.

In the training phase, the images were randomly resized in a scale of $[0.8, 1]$, while the validation images were resized such that their smallest dimension was 256 pixels and their original aspect ratio was retained. For the ResNet152 backbone, random crops of 224×224 pixels were extracted and randomly flipped horizontally. In the testing phase, following Huang et al. [18], we applied 20 random crops and averaged the resulting image embeddings. For the Attention-based VSRN [20] backbone¹, we applied the Faster RCNN to generate 36 ROIs per image in both training and testing, and the images were augmented in the training phase by horizontal flipping. Following [19], [20], the resulting VSRN-based model is an ensemble computed by averaging the output embeddings of the three models which performed best on the validation set. For both backbones, the mean of each color channel was subtracted. In the text branch, the captions were tokenized using the vocabulary provided by Faghri et al. [13] such that each sentence was encoded by a vector of tokens.

In the image annotation tasks, we computed the distance between the embedding of the query image and the embeddings of all captions in the dataset. The captions were ranked according to the minimal distance. Similarly, in the image search task, we computed the distance between the embedding of the query caption and the embeddings of all images in the dataset. The distance was then used to rank the similarity.

As in previous works, we quantify the retrieval accuracy by R@K, which is “the recall at K ” – the fraction of queries in which a correct item is retrieved within the K embeddings closest to the query. We consider two retrieval tasks. The first is *image annotation* (Img2Txt), where given a query image, we aim to retrieve the corresponding captions, while the second is the *image search* (Txt2Img) task, where given a text query (caption) we search for the corresponding image. Thus, an image annotation recall rate at K (R@K), is the average number of accurate captions retrieved, within the K captions nearest to the query image. Similarly, an image search recall rate of K (R@K) is the average number of accurate images retrieved, given a text query, within the K most similar images.

4.1 Training

All CNN models were trained in two phases: first, computing the unquantized embedding (Section 3.3), and then refining the resulting CNN to compute the quantized embedding (Section 3.4). The *unquantized* embedding was computed using a precomputed image embedding CNN, where the succeeding layers were trained by applying the Center Loss in Eq. 6 and the adaptive hinge loss (Section 3.5). The training samples $\{s_n\}_1^N$ were assigned to the unquantized semantic centers $\{c_n\}_1^N$, such that s_n is assigned to c_n . The input to this training phase is a batch of pairs of corresponding images and captions that are used as positive pairs. The negative pairs are assigned by matching an image to randomly chosen caption within the batch. The network is trained by optimizing Eq. 5. The cross-entropy losses are trained using the labels of the subsets $S = \{s_n\}_1^N$, as in Section 3. Thus, the image \mathbf{x}_n and captions $\mathbf{y}_n^1, \dots, \mathbf{y}_n^K$ in a subset $s_n = \{\mathbf{x}_n, \mathbf{y}_n^1, \dots, \mathbf{y}_n^K\}$ are labeled by n .

Next, we trained the *quantized* embedding $C_q = \{\hat{c}_n\}_1^{N_q}$, by adding the “ N_q FC” and Softmax layers as in Fig. 2. As the layer “ N_q FC” is uninitialized, it is first trained by freezing all other CNN layers until convergence. We then unfroze all layers and fine-tuned the network end-to-end. The quantized centers $\{\hat{c}_n\}_1^{N_q}$ were *initialized* by applying KMEANS with N_q centers to $\{c_n\}_1^N$. We also tried using a random initialization of $\{\hat{c}_n\}_1^{N_q}$, and got similar results, but a longer convergence. The cross-entropy losses in this phase, are as in the first phase.

Layer	Output
ResNet152 conv1 block	$112 \times 112 \times 64$
ResNet152 conv2.x block	$56 \times 56 \times 256$
ResNet152 conv3.x block	$28 \times 28 \times 512$
ResNet152 conv4.x block	$14 \times 14 \times 1024$
ResNet152 conv5.x block	$7 \times 7 \times 2048$
AveragePooling	1×2048
L2 Normalization	1×2048
FC	1×1024
L2 Normalization	1×1024
FC (softmax)	$1 \times \#\text{semantic concepts}$

TABLE 1

The layers of the image embedding branch corresponding to \mathbf{H}_1 , as depicted in Fig. 2.

The Adam optimizer [40] was used to optimize the parameters of both image and text branches with a varying learning rate starting at $2 \cdot 10^{-4}$ for the first phase, and

1. <https://github.com/KunpengLi1994/VSRN>

Layer	Output
Embedding	#tokens \times 300
Bi-Directional GRU	1×1024
L2 Normalization	1×1024
FC (softmax)	$1 \times \#semantic\ concepts$

TABLE 2

The layers of the text embedding branch corresponding to \mathbf{H}_t , as depicted in Fig. 2.

$2 \cdot 10^{-5}$ for the second and third phases. The SGD optimizer was used to optimize the Semantic Center Loss parameters using a learning rate of 0.5, where we reduced the learning rates by a factor of 0.1 every 15 epochs. We trained the first phase for 30 epochs, the second phase for an additional 15 epochs, and the third phase for 10 epochs. A fixed margin of $m_x = m_y = 0.2$ was set for the hinge loss in the first and second training phases, and both margins were optimized in the third phase. We apply the proposed adaptive hinge loss to $\hat{\mathbf{x}}$ and $\hat{\mathbf{y}}$, as in Eq. 13, by accumulating the statistics M_x and M_y over $q = 500$ iterations, and update the margins m_x and m_y using the multiplier $c = 1.03$, if more than $r = 0.8$ of the negative margins are beyond the hinge loss margins M_x and M_y . These settings were applied to training the models for all datasets.

As the proposed scheme can be used with any text and image embedding CNNs, we applied it to two image-text matching CNNs. The first is detailed in Tables 1 and 2 (ResNet-based), and the second is based on the VSRN [20] approach².

4.2 Flickr30K Results

The proposed scheme was also evaluated using the Flickr30K [5] dataset and was compared with multiple state-of-the-art schemes [10], [13], [14], [15], [16], [18], [19], [20]. The Flickr30K dataset consists of 31,000 Flickr images, each having five captions, and following Karpathy and Fei-Fei [4], we used 1,000 images (and corresponding captions) for validation, 1,000 images for testing and the rest for training. In the first phase of the training, we used a batch size of 128 samples. We applied the proposed scheme using both the VSRN [20] and the CNN in Tables 1 and 2, as a backbone for feature extraction. The ResNet-based results are reported in the upper part of Table 3, where the proposed scheme implemented using 1000 quantization centers, outperforms all previous schemes using the same backbone, in all categories, by an average of 3.3%.

The lower part of Table 3 reports the results for the SCAN [19] and VSRN [20] schemes. Both of these schemes utilize an ensemble consisting of two CNNs trained independently, where the similarity results are averaged. Thus, in these schemes, multiple CNNs were trained, and the optimal ensemble is chosen according to their joint evaluation score on the validation set. We trained two CNNs based on the VSRN backbone using 1000 quantization centers. It follows that each of our CNNs outperforms the VSRN [20] and SCAN [19] in 6/6 and 5/6 categories, respectively. Training additional models from which to choose the ensemble can improve our ensembles's accuracy.

2. Available at: <https://github.com/KunpengLi1994/VSRN>

Model	Annotation			Search		
	r@1	r@5	r@10	r@1	r@5	r@10
VGG19						
Embedd [16]	40.7	-	79.2	29.2	-	71.7
smLSTM [15]	42.5	71.9	81.5	30.2	60.4	72.3
2Way [10]	49.8	67.5	-	36.0	55.6	-
ResNet152						
DAN [14]	55.0	-	89.0	39.4	-	79.1
VSE++ [13]	52.9	79.1	87.2	39.6	69.6	79.5
Ours	58.6	84.4	91.1	45.5	75.2	83.9
Attention-based						
Huang [18]	55.5	82.0	89.3	41.1	70.5	80.1
SCAN [19]	67.4	90.3	95.8	48.6	77.7	85.2
VSRN [20]	71.3	90.6	96.0	54.7	81.8	88.2
Ours	73.3	92.2	96.0	57.0	82.8	89.2

TABLE 3

The Accuracy of the image annotation and search tasks evaluated using the **Flickr30K dataset**. The center loss was applied to the image and text embeddings as a semantic embedding. We also applied the Triplet Hinge Loss with an Adaptive Margins, as in Section 3.5.

Qualitative retrieval results are shown in Figs. 3 and 4, while an example of a failed image annotation task is shown in Fig. 5. These are the images whose embedding is the closest to embedding of the query. By examining the failed retrieval, it follows that although the retrieved captions are not part of the groundtruth captions, are semantic similar to the query. Similarly, in Fig. 3, the correct image is indeed retrieved first (shown on the upper-left corner), but the following five retrieved images are also related to the “karate hat” query.

Girl about to kick a piece of wood in half while karate instructor holds it



Fig. 3. Image search (text to image retrieval) example taken from the **Flickr30K** dataset. The query caption appears on top of the images. The text embedding was compared to the embeddings of all of the images in the dataset. The ten top ranked images are presented. The retrieved images are depicted according to their similarity: left-to-right and then top-down. The most similar image in on the upper-left corner, and is the correct retrieval result.

4.3 MS-COCO Results

The MS-COCO [23] dataset is significantly larger than the Flickr8K and Flickr30K datasets and was split to 5000 images for test, 5000 images for validation, while the remaining 113,287 images were used for training, following Karpathy and Fei-Fei [4]. In the first phase of the training, we used a batch size of 128, while in the second and third phases, we applied a batch size of 64. Due to the large number



1. **The man with pierced ears is wearing glasses and an orange hat.**
2. **A man wears an orange hat and glasses.**
3. **A man with gauges and glasses is wearing a Blitz hat.**
4. A man wearing a helmet and sunglasses smiles.
5. A man wearing a white t-shirt has his mouth open wide.
6. A man wearing a tank-top and a baseball cap holding a camera.
7. A man smiling with a helmet on his head.
8. **A man with glasses is wearing a beer can crocheted hat.**
9. **A man in an orange hat staring at something.**
10. A man share a Carlsberg toast with someone.

Fig. 4. Image annotation (image to text retrieval) example taken from the **Flickr30K** dataset. The image embedding was compared to the embeddings of all captions in the dataset. The ten top ranked captions are presented, and the correctly retrieved ones are marked in **bold**.



1. Several workers wearing hard hats dig a hole.
2. Three construction workers are digging a whole next to a wall in a field.
3. Four workmen removing debris, from a hole in the ground.
4. Three men with hard hats in front of a large hole in the ground.
5. Four construction workers gathered around a hole looking in a bucket.
6. Several construction workers with orange safety vests are digging into the ground.
7. The workers are surrounding a hole with a bucket.
8. Kids scale a wall as two other people watch.
9. Two children climb a rock wall as two people watch carefully.
10. Construction workers picketing against PM Construction Services.

Fig. 5. An example of a failed image annotation (image to text retrieval) taken from the **Flickr30K** dataset. The top ten retrieval results bear partial semantic similarity to the image content.

of training images, we applied the quantized semantic loss introduced in Section 3.4, using 1000 quantized semantic centers. We report the results of two test setups: In the first, reported in Table 4, the 5000 test images were split into five sets of 1000 images (and captions), and the results are averaged over the five folds (COCO1K). In the second, reported in Table 5, the results of the 5000 test images are averaged as a single test set (COCO5K). Same as in the previous datasets, we trained different CNNs using the VSRN [20] and ResNet backbones. For the COCO1K, we outperform the SCAN and VSRN schemes in *all* categories. For the COCO5K dataset, our approach outperformed the previous best ResNet-based approaches (Huang [18]) in 5/6 categories, by an average of 1.5%. Comparing the accuracy for the Flickr8K, Flickr30K and MS-COCO in Tables 6, 3 and

Model	Annotation			Search		
	r@1	r@5	r@10	r@1	r@5	r@10
VGG19						
Embedd [16]	50.4	-	69.4	39.8	-	86.6
sm-LSTM [15]	53.2	83.1	91.5	40.7	75.8	87.4
2WayNet [10]	55.8	75.2	-	39.7	63.3	-
ResNet152						
VSE++ [13]	64.6	89.1	95.7	52.0	83.1	92.0
Ours	69.3	93.2	97.7	56.0	86.6	93.7
Attention-based						
Huang [18]	69.9	92.9	97.5	56.7	87.5	94.8
SCAN [19]	72.7	94.8	98.4	58.8	88.4	94.8
VSRN [20]	76.2	94.8	98.2	62.8	89.7	95.1
Ours	76.6	95.6	98.6	63.9	90.3	95.4

TABLE 4

The Accuracy of the image annotation and search tasks evaluated using the **MS-COCO dataset 1K test**. The center loss was applied to the image and text embeddings as a semantic embedding.

5, respectively, it follows that training the proposed scheme on larger datasets consistently improves the retrieval accuracy.

Model	Annotation			Search		
	r@1	r@5	r@10	r@1	r@5	r@10
VGG19						
Embedd [16]	50.4	-	69.4	39.8	-	86.6
smLSTM [15]	53.2	83.1	91.5	40.7	75.8	87.4
2WayNet [10]	55.8	75.2	-	39.7	63.3	-
ResNet152						
VSE++ [13]	41.3	69.2	81.2	30.3	59.1	72.4
Huang [18]	42.8	72.3	83.0	33.1	62.9	75.5
Ours	44.7	75.4	86.0	33.1	63.7	75.8

TABLE 5

The Accuracy of the image annotation and search tasks evaluated using the **MS-COCO dataset 5K test**. The center loss was applied to the image and text embeddings as a semantic embedding.

Qualitative retrieval results are shown in Figs. 6 and 7, while an image annotation failure is shown in Fig. 8.



1. Several giraffes eating leaves from the ground and tree.
2. **Giraffes are feeding on the trees and grass.**
3. Several giraffe eating the leaves from neighboring trees.
4. Two giraffes in a wild, lightly wooded field.
5. **A giraffe grazing on a tree in the wilderness with other wildlife.**
6. Two giraffe standing next to each other in a forest.
7. Two giraffes are standing in the middle of some vegetation.
8. A group of giraffes that are in the dirt.
9. A giraffe is walking through the forest with tall trees.
10. Two giraffes standing in a brush covered area.

Fig. 6. Image annotation (image to text retrieval) example taken from the **MS-COCO** dataset. The image embedding was compared to the embeddings of all captions in the dataset. The ten top ranked captions are presented, and the correctly retrieved ones are marked in **bold**.

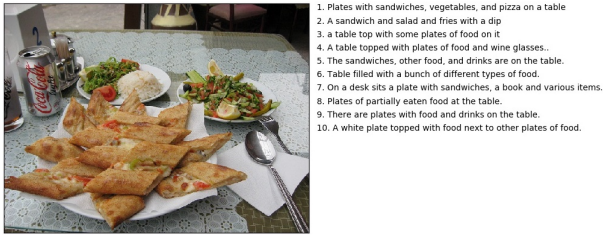
Man riding a motor bike on a dirt road on the countryside.



Fig. 7. Image search (text to image retrieval) example taken from the **MS-COCO** dataset. The query caption appears on top of the images. The text embedding was compared to the embeddings of all of the images in the dataset. The ten top ranked images are presented. The retrieved images are depicted according to their similarity: left-to-right and then top-down. The most similar image is on the upper-left corner, and is the correct result.

4.4 Flickr8K Results

We applied the proposed scheme to the Flickr8K [22] dataset, which was split to 1000 images (and corresponding captions) for test, 1000 images for validation, and 6000 images for training, following Karpathy and Fei-Fei [4]. We used a batch size of 128, and applied the proposed semantic embedding to two backbones: the one in Tables



1. Plates with sandwiches, vegetables, and pizza on a table
2. A sandwich and salad and fries with a dip
3. a table top with some plates of food on it
4. A table topped with plates of food and wine glasses.
5. The sandwiches, other food, and drinks are on the table.
6. Table filled with a bunch of different types of food.
7. On a desk sits a plate with sandwiches, a book and various items.
8. Plates of partially eaten food at the table.
9. There are plates with food and drinks on the table.
10. A white plate topped with food next to other plates of food.

Fig. 8. An example of failed image annotation (image to text retrieval) taken from the **MS-COCO** dataset. The top ten retrieval results bear partial semantic similarity to the image content.

Model	Annotation		Search	
	r@1	r@5	r@1	r@5
CCA [8]	31.0	59.3	21.3	50.1
RNN-FV [41]	31.6	61.2	23.2	53.3
VQA-A [42]	24.3	52.2	17.2	42.8
2WayNet [10]	43.4	63.2	29.3	49.7
Ours 50c	38.9	67.9	29.2	59.6
Ours 100c	44.1	69.7	29.9	59.7
Ours 1000c	39.2	67.8	29.4	59.3
Ours 6000c	38.6	68.3	29.9	60.3
VSRN [20]				
VSRN	42.5	73.9	33.5	64.2
Ours 1000c	42.9	74.3	34.3	64.7

TABLE 6

The accuracy of the image annotation and search tasks evaluated using the **Flickr8K** dataset. The center loss was applied to the image and text embeddings as a semantic embedding. We also applied the Triplet Hinge Loss with Adaptive Margins, as in Section 3.5.

1, 2, and the one based on the VSRN [20] approach. The retrieval results are reported in Table 6, where we separately compare the results of CNN trained with different backbones. It follows that the proposed approach outperforms all previous schemes in general, and improves over the VSRN [20] and other backbones by an average of 0.6% and 4.5%, respectively. As for the number of centers, we tested several configurations and the ‘sweet spot’ of 100 centers performs best, on both validation and test sets. Qualitative examples are shown in Figs. 9 and 11, where an image annotation failure is shown in Fig. 10. We note that although the caption retrieved first in Fig. 10 is incorrect, it seems to adhere to the caption.



1. A Sooners football player was the number 28 and black armbands .
2. A Oklahoma Sooners football player wearing his jersey number 28 .
3. The red and white football team is talking with the officials .
4. A man is wearing a Sooners red football shirt and helmet .
5. A football player wearing an orange uniform smiling and holding the football .
6. Oklahoma University football players in front of a crowd of Sooners fans and next to three referees .
7. A Sooners football player moves quickly on the field as another player runs .
8. A football player in red and white is talking to a coach .
9. A football player wearing an orange jersey holding a football
10. Football players gather around the referees .

Fig. 9. Image annotation (image to text retrieval) example taken from the **Flickr8K** dataset. The image embedding was compared to the embeddings of all captions in the dataset. The ten top ranked captions are presented, and the correctly retrieved ones are marked in **bold**.



1. A beige dog with orange vest running on withering grass .
2. A little tan dog with large ears running through the grass .
3. A yellow lab jumping up to catch a toy .
4. A tan dog and a cream colored dog run through grasslands .
5. A big dog chases a little dog on the grass .
6. The yellow dog is trying to catch a red Frisbee .
7. A brown and tan dog walks through the green grass .
8. The white dog is running in the green grass .
9. a dog runs through the long grass .
10. The white dog is chasing a toy that is attached to a string across the grass .

Fig. 10. An example of failed image annotation (image to text retrieval) taken from the **Flickr8K** dataset. The top ten retrieval results bear partial semantic similarity to the image content.

A yellow dog is playing in a grassy area near flowers .



Fig. 11. Image search (text to image retrieval) example taken from the **Flickr8K** dataset. The query caption appears on top of the images. The text embedding was compared to the embeddings of all of the images in the dataset. The ten top ranked images are presented. The retrieved images are depicted according to their similarity: left-to-right and then top-down. The reference result is marked by *. It seems that the leading retrieval result (top-left) corresponds to the given caption as well.

4.5 Ablation study

We conducted an ablation study to evaluate the influence and importance of the multiple algorithmic components of the proposed scheme. We first studied the use of the Cross Entropy losses (as in Fig. 2) and the proposed Semantic Centers formulation. For that, we applied different combinations of these losses to the Flickr8K and Flickr30K datasets. The Center loss was applied in an unquantized formulation, and the results are shown in Tables 7. Using the Semantic Center loss (without the Cross Entropy losses) provides an average accuracy improvement of 19.3% and 2.5%, when applied to the Flickr8K and Flickr30K datasets, respectively, compared to applying the Center loss to the text embeddings only. In contrast, applying the Cross Entropy losses, alongside the semantic losses, provides an average improvement of only 0.3%. Hence, the proposed Semantic Center loss is the one doing the heavy lifting in our scheme.

In Table 8, we compared using the unquantized and quantized Semantic Center losses (with 1000 centers) to a baseline without the Center Loss. For that we applied the Resnet152 [13], [14] and VSRN [20] backbones to the Flickr30K dataset. For the Resnet152 backbone, without using the random crops, the Center loss outperformed the baseline by 2.5%. In contrast, when random crops were used, the average improvement of the Center loss was only

Model		Annotation		Search	
Centers	CE loss	r@1	r@10	r@1	r@10
Flickr8K					
Txt	-	6.6	33.9	15.7	53.6
Txt	Txt	9.7	42.1	15.3	53.8
Semantic	-	30.1	73.6	21.6	61.9
Semantic	Img/Txt	32.3	71.6	22.1	63.4
Flickr30K					
Txt	-	43.9	81.2	30.9	71.9
Txt	Txt	45.1	82.6	32.5	72.9
Semantic	-	46.7	83.4	33.7	74.0
Semantic	Img/Txt	46.9	84.0	33.3	73.8

TABLE 7

Ablation study of the Semantic Centers, and the Cross-Entropy (CE) losses, using the Flickr8K and Flickr30K datasets. The Center loss is applied to either the text embeddings (txt), or as Semantic centers (Semantic) to both the text and image embeddings.

0.8%. Using the random crops improved the accuracy by 2%. In contrast, applying the VSRN backbone improves the overall average accuracy by a significant 6% and the average improvement of the Center loss is 0.8%. It seems that as the backbone CNN becomes more elaborate (VSRN vs. Resnet152), the available margin for improvement reduces. Still, the improvement achieved by the Center loss is complementary to improving the backbone.

Center Loss	Annotation			Search		
	r@1	r@5	r@10	r@1	r@5	r@10
Resnet152 backbone - No Random Crops						
No	52.9	79.1	87.2	39.6	69.6	79.5
Unquantized	55.8	82.5	89.3	41.8	71.5	79.9
Quantized	57.2	83.6	89.3	42.3	72.0	80.3
Resnet152 backbone - With Random Crops						
No	57.1	85.2	91.5	41.9	72.3	82.2
Unquantized	59.9	83.9	90.8	43.9	73.5	81.8
Quantized	60.1	83.7	91.9	44.6	73.9	82.5
VSRN backbone- No ensemble						
No	68.1	89.5	94.2	50.5	78.8	86.4
Unquantized	68.3	90.4	94.9	51.9	80.2	87.0
Quantized	69.8	88.7	94.6	52.2	79.8	87.0

TABLE 8

An ablation study of the configurations of the Semantic Center loss. The schemes were applied to the Flickr30K dataset, using 1000 quantized Semantic centers.

The sensitivity to the number of Semantic Centers is studied in Table 9, where we applied varying numbers of centers to the Flickr8K, Flickr30K and MS-COCO1K datasets. We computed the maximal difference in average accuracy, that was 1% for the Flickr8K, in contrast to 0.1% for the Flickr30K and MS-COCO1K datasets. This implies that the choice of the number of centers is robust.

We also studied using a Transformer-based text embedding, instead of the embedding layer-based embedding used in previous works [13], [18], [19], [20]. For that we applied the pretrained “bert-large-uncased” model by Huggingface³. The model was fine-tuned by setting its learning-rate to 10^{-5} . The results are shown in Table 10, where the use of the Bert-based language model improved the retrieval accuracy by an average of 1%. This is an insignificant improvement considering the huge number of parameters (336M parameters). It seems that due to the relatively lim-

3. <https://huggingface.co/bert-large-uncased>

#Centers	Annotation			Search		
	r@1	r@5	r@10	r@1	r@5	r@10
Flickr 8K						
50	38.9	67.9	-	29.2	59.6	-
100	44.1	69.7	-	29.9	59.7	-
1000	39.2	67.8	-	29.4	59.3	-
Flickr 30K						
100	56.7	83.4	89.8	42.1	71.9	80.3
500	57.8	82.9	89.8	42.0	72.1	80.2
1000	57.2	83.6	89.3	42.3	72.0	80.3
5000	57.3	82.9	90.0	41.8	71.9	80.0
MS-COCO 1K						
500	66.5	91.6	96.7	53.8	85.0	92.6
1000	66.5	91.4	96.6	53.9	85.1	92.6
5000	66.7	91.2	96.7	53.9	85.0	92.6

TABLE 9

Ablation study results for number of centers for the quantization phase. We used a ResNet152 backbone for these results, and the Flickr 30K and MS-COCO were tested without random crops.

ited vocabulary of the captions and their short length, a simple language model based on learnt embeddings is able to perform well.

Text embedding	Annotation			Search		
	r@1	r@5	r@10	r@1	r@5	r@10
Resnet152 backbone - With Random Crops						
Embedding	60.1	83.7	91.9	44.6	73.9	82.5
Transformer	60.4	84.2	92.8	45.5	74.1	83.4
VSRN backbone- No ensemble						
Embedding	69.8	88.7	94.6	52.2	79.8	87.0
Transformer	70.6	89.1	95.4	52.3	80.2	87.9

TABLE 10

An ablation study of the text embedding. We compare using learnt embeddings and the “bert-large-uncased” Transformer-based language model by Huggingface. The schemes were applied to the Flickr30K dataset, using 1000 quantized Semantic centers.

We also examined the effectiveness of the proposed adaptive margin scheme introduced in Section 3.5. For that we applied the proposed scheme to the Flickr30K dataset using different values of the scaling factor c defined in Eq. 13. We also compare to using the adaptive margins proposed by Wu et al. [33] and Li [35]. The choice of c seems to be robust. Choosing $c \in [1.03, 1.05]$ provides an accuracy improvement of 0.7%, while outperforming the Adaptive Margin schemes by Wu [33] and Li [35] by close to 25% and 15%, respectively.

Adaptive Margin	c	Annotation			Search			Avg.
		r@1	r@5	r@10	r@1	r@5	r@10	
Non	-	55.8	82.5	89.3	41.8	71.5	79.9	70.1
Our	1.10	55.9	80.6	89.2	41.9	71.8	80.6	70.0
Our	1.05	57.7	82.8	89.1	41.4	70.9	80.2	70.4
Our	1.03	57.0	82.7	89.9	42.1	71.8	80.5	70.7
Wu [33]	-	28.6	54.8	65.8	19.1	44.1	54.9	44.6
Li [35]	-	47.6	69.3	75.8	24.6	53.7	64.4	55.9

TABLE 11

Ablation study of the proposed adaptive margin, evaluated using the Flickr30K dataset. We compare with the adaptive margins scheme by Wu et al. [33].

5 CONCLUSIONS

In this work, we proposed an approach for computing joint image-text embeddings that encode the semantic similarity

in a Euclidean L_2 space. For that, we first applied the semantic center loss to encode *identical* semantic concepts based on the training set. By introducing a differentiable quantization into the end-to-end trainable network, we derive an embedding that encodes semantic *similarity*. The similarity is thus encoded automatically, without having to define the similar concepts explicitly, based on textual analysis, as in previous works. We also propose a novel formulation of the triplet loss using adaptive hinge loss margins that are updated continuously throughout the training, allowing improved retrieval accuracy. The proposed contributions can be applied to *any* CNN subnetworks for text and image embedding such as the ResNet152 CNN and GRU, or VSRN [20] used in this implementation. Our scheme is experimentally shown to compare favorably with contemporary state-of-the-art approaches when applied to multiple image-text datasets.

REFERENCES

- [1] M. Malinowski, M. Rohrbach, and M. Fritz, "Ask your neurons: A neural-based approach to answering questions about images," in *2015 IEEE International Conference on Computer Vision (ICCV)*, 2015, pp. 1–9.
- [2] M. Tanti, A. Gatt, and K. Camilleri, "What is the role of recurrent neural networks (rnns) in an image caption generator?" in *Proceedings of the 10th International Conference on Natural Language Generation*. Association for Computational Linguistics, 2017, pp. 51–60.
- [3] R. Kiros, R. Salakhutdinov, and R. S. Zemel, "Unifying Visual-Semantic Embeddings with Multimodal Neural Language Models," *ArXiv e-prints*, Nov. 2014.
- [4] A. Karpathy and L. Fei-Fei, "Deep visual-semantic alignments for generating image descriptions," *IEEE Trans. Pattern Anal. Mach. Intell.*, vol. 39, no. 4, pp. 664–676, Apr. 2017.
- [5] P. Young, A. Lai, M. Hodosh, and J. Hockenmaier, "From image descriptions to visual denotations: New similarity metrics for semantic inference over event descriptions," *Transactions of the Association for Computational Linguistics*, vol. 2, pp. 67–78, 2014.
- [6] K. Q. Weinberger, J. Blitzer, and L. K. Saul, "Distance metric learning for large margin nearest neighbor classification," in *Proceedings of the 18th International Conference on Neural Information Processing Systems*, ser. NIPS'05. Cambridge, MA, USA: MIT Press, 2005, pp. 1473–1480.
- [7] J. Goldberger, G. E. Hinton, S. T. Roweis, and R. R. Salakhutdinov, "Neighbourhood components analysis," in *Advances in Neural Information Processing Systems 17*, L. K. Saul, Y. Weiss, and L. Bottou, Eds. MIT Press, 2005, pp. 513–520.
- [8] B. Klein, G. Lev, G. Sadeh, and L. Wolf, "Associating neural word embeddings with deep image representations using fisher vectors," in *2015 IEEE Conference on Computer Vision and Pattern Recognition (CVPR)*, June 2015, pp. 4437–4446.
- [9] S. Akaho, "A kernel method for canonical correlation analysis," *eprint arXiv:cs/0609071*, Sep. 2006.
- [10] A. Eisenschadt and L. Wolf, "Linking Image and Text with 2-Way Nets," *2017 IEEE Conference on Computer Vision and Pattern Recognition (CVPR)*, pp. 1855–1865, 2017.
- [11] G. Andrew, R. Arora, J. Bilmes, and K. Livescu, "Deep canonical correlation analysis," in *Proceedings of the 30th International Conference on International Conference on Machine Learning - Volume 28*, ser. ICML'13. JMLR.org, 2013, pp. III-1247–III-1255.
- [12] S. Chandar, M. M. Khapra, H. Larochelle, and B. Ravindran, "Correlational neural networks," *Neural Computation*, vol. 28, no. 2, pp. 257–285, 2016.
- [13] F. Faghri, D. J. Fleet, J. R. Kiros, and S. Fidler, "Vse++: Improving visual-semantic embeddings with hard negatives," *Proceedings of the British Machine Vision Conference (BMVC)*, 2018.
- [14] "Dual attention networks for multimodal reasoning and matching," in *2017 IEEE Conference on Computer Vision and Pattern Recognition, CVPR 2017, Honolulu, HI, USA, July 21-26, 2017*. IEEE Computer Society, 2017, pp. 2156–2164.
- [15] Y. Huang, W. Wang, and L. Wang, "Instance-aware Image and Sentence Matching with Selective Multimodal LSTM," *2017 IEEE Conference on Computer Vision and Pattern Recognition (CVPR)*, 2017.
- [16] L. Wang, Y. Li, J. Huang, and S. Lazebnik, "Learning two-branch neural networks for image-text matching tasks," *IEEE Trans. Pattern Anal. Mach. Intell.*, vol. 41, no. 2, pp. 394–407, 2019.
- [17] A. Frome, Y. Singer, F. Sha, and J. Malik, "Learning globally-consistent local distance functions for shape-based image retrieval and classification," in *2007 IEEE 11th International Conference on Computer Vision*, Oct 2007, pp. 1–8.
- [18] Y. Huang, Q. Wu, and L. Wang, "Learning semantic concepts and order for image and sentence matching," *2018 IEEE Conference on Computer Vision and Pattern Recognition*, pp. 6163–6171, 2018.
- [19] K. Lee, X. Chen, G. Hua, H. Hu, and X. He, "Stacked cross attention for image-text matching," in *Computer Vision - ECCV 2018 - 15th European Conference, Munich, Germany, September 8-14, 2018, Proceedings, Part IV*, 2018, pp. 212–228.
- [20] K. Li, Y. Zhang, K. Li, Y. Li, and Y. Fu, "Visual semantic reasoning for image-text matching," in *Proceedings of the 2019 IEEE International Conference on Computer Vision (ICCV)*, ser. ICCV '19. IEEE Computer Society, 2019.
- [21] S. Ren, K. He, R. Girshick, and J. Sun, "Faster R-CNN: Towards real-time object detection with region proposal networks," in *Advances in Neural Information Processing Systems 28*, C. Cortes, N. D. Lawrence, D. D. Lee, M. Sugiyama, and R. Garnett, Eds. Curran Associates, Inc., 2015, pp. 91–99.
- [22] M. Hodosh, P. Young, and J. Hockenmaier, "Framing image description as a ranking task: Data, models and evaluation metrics," *J. Artif. Int. Res.*, vol. 47, no. 1, pp. 853–899, May 2013.
- [23] T.-Y. Lin, M. Maire, S. Belongie, J. Hays, P. Perona, D. Ramanan, P. Dollár, and C. L. Zitnick, "Microsoft coco: Common objects in context," in *Computer Vision - ECCV 2014*, D. Fleet, T. Pajdla, B. Schiele, and T. Tuytelaars, Eds. Cham: Springer International Publishing, 2014, pp. 740–755.
- [24] A. Li, S. Shan, X. Chen, and W. Gao, "Maximizing intra-individual correlations for face recognition across pose differences," in *2009 IEEE Conference on Computer Vision and Pattern Recognition*, June 2009, pp. 605–611.
- [25] W. Wang, R. Arora, K. Livescu, and J. Bilmes, "On deep multi-view representation learning," in *Proceedings of the 32nd International Conference on International Conference on Machine Learning - Volume 37*, ser. ICML'15. JMLR.org, 2015, p. 1083–1092.
- [26] G. Chechik, V. Sharma, U. Shalit, and S. Bengio, "Large scale online learning of image similarity through ranking," *J. Mach. Learn. Res.*, vol. 11, pp. 1109–1135, Mar. 2010.
- [27] M. Norouzi and D. J. Fleet, "Minimal loss hashing for compact binary codes," in *Proceedings of the 28th International Conference on International Conference on Machine Learning*, ser. ICML'11. USA: Omnipress, 2011, pp. 353–360.
- [28] J. Weston, S. Bengio, and N. Usunier, "Wsbie: Scaling up to large vocabulary image annotation," in *Proceedings of the Twenty-Second International Joint Conference on Artificial Intelligence - Volume Three*, ser. IJCAI'11. AAAI Press, 2011, pp. 2764–2770.
- [29] A. Frome, G. S. Corrado, J. Shlens, S. Bengio, J. Dean, M. A. Ranzato, and T. Mikolov, "Devise: A deep visual-semantic embedding model," in *Advances in Neural Information Processing Systems 26*, 2013, pp. 2121–2129.
- [30] R. Socher, A. Karpathy, Q. V. Le, C. D. Manning, and A. Y. Ng, "Grounded compositional semantics for finding and describing images with sentences," *Transactions of the Association for Computational Linguistics*, 2013.
- [31] A. Jabri, A. Joulin, and L. van der Maaten, "Revisiting visual question answering baselines," in *Computer Vision - ECCV 2016 - 14th European Conference, Amsterdam, The Netherlands, October 11-14, 2016, Proceedings, Part VIII*, ser. Lecture Notes in Computer Science, B. Leibe, J. Matas, N. Sebe, and M. Welling, Eds., vol. 9912. Springer, 2016, pp. 727–739.
- [32] J. L. Ba, K. Swersky, S. Fidler, and R. Salakhutdinov, "Predicting deep zero-shot convolutional neural networks using textual descriptions," in *2015 IEEE International Conference on Computer Vision (ICCV)*, Dec 2015, pp. 4247–4255.
- [33] R. Manmatha, C. Wu, A. J. Smola, and P. Krähenbühl, "Sampling matters in deep embedding learning," in *IEEE International Conference on Computer Vision, ICCV 2017, Venice, Italy, October 22-29, 2017*. IEEE Computer Society, 2017, pp. 2859–2867.
- [34] W. Chen, X. Chen, J. Zhang, and K. Huang, "Beyond triplet loss: A deep quadruplet network for person re-identification," in *2017*

IEEE Conference on Computer Vision and Pattern Recognition (CVPR), 2017, pp. 1320–1329.

- [35] A. Li, W. Huang, X. Lan, J. Feng, Z. Li, and L. Wang, “Boosting few-shot learning with adaptive margin loss,” in *Proceedings of the IEEE/CVF Conference on Computer Vision and Pattern Recognition (CVPR)*, June 2020.
- [36] M. Patrick, P.-Y. Huang, Y. M. Asano, F. Metze, A. Hauptmann, J. Henriques, and A. Vedaldi, “Support-set bottlenecks for video-text representation learning,” in *International Conference on Learning Representations (ICLR)*, 2021.
- [37] Y. Wen, K. Zhang, Z. Li, and Y. Qiao, “A discriminative feature learning approach for deep face recognition,” in *Computer Vision - ECCV 2016 - 14th European Conference, Amsterdam, The Netherlands, October 11-14, 2016, Proceedings, Part VII*, 2016, pp. 499–515.
- [38] R. Arandjelović, P. Gronat, A. Torii, T. Pajdla, and J. Sivic, “NetVLAD: CNN architecture for weakly supervised place recognition,” in *IEEE Conference on Computer Vision and Pattern Recognition*, 2016.
- [39] B. D. Brabandere, D. Neven, and L. V. Gool, “Semantic instance segmentation with a discriminative loss function,” *CoRR*, vol. abs/1708.02551, 2017. [Online]. Available: <http://arxiv.org/abs/1708.02551>
- [40] D. P. Kingma and J. Ba, “Adam: A method for stochastic optimization,” in *3rd International Conference on Learning Representations, ICLR 2015, San Diego, CA, USA, May 7-9, 2015, Conference Track Proceedings*, Y. Bengio and Y. LeCun, Eds., 2015.
- [41] G. Lev, G. Sadeh, B. Klein, and L. Wolf, “RNN fisher vectors for action recognition and image annotation,” in *Computer Vision – ECCV 2016*, B. Leibe, J. Matas, N. Sebe, and M. Welling, Eds. Cham: Springer International Publishing, 2016, pp. 833–850.
- [42] X. Lin and D. Parikh, “Leveraging visual question answering for image-caption ranking,” in *Computer Vision - ECCV 2016 - 14th European Conference, Amsterdam, The Netherlands, October 11-14, 2016, Proceedings, Part II*, ser. Lecture Notes in Computer Science, B. Leibe, J. Matas, N. Sebe, and M. Welling, Eds., vol. 9906. Springer, 2016, pp. 261–277.



Noam Malali earned a B.Sc. and an M.Sc. in electrical engineering from Bar-Ilan University in 2011 and 2020, respectively. His research interests center on deep learning and machine learning. Expert in applied machine learning, he has broad experience in many areas of research in the hi-tech industry and academia.



Yosi Keller Yosi earned his BSc in electrical engineering from Technion-Israel Institute of Technology, Haifa, in 1994, and his MSc and Ph.D. degrees in electrical engineering from Tel Aviv University, summa cum laude, in 1998 and 2003, respectively. He was a Gibbs Assistant Professor at Yale University from 2003 to 2006. He is an Associate Professor at the Faculty of Engineering at Bar Ilan University in Ramat-Gan, Israel. His research interests are in Computer Vision, Deep Learning, and Biometrics.